Title

Reaction Dynamics in Polyatomic Molecular Systems: Some Approaches for Constructing Potential Energy Surfaces and Incorporating Quantum Effects in Classical Trajectory Simulations

Author

Miller, W.H.

Publication Date

1992

LBL-31626

Lawrence Berkeley Laboratory
UNIVERSITY OF CALIFORNIA

Materials & Chemical
Sciences Division

To be published as a chapter in *The Role of Computational Models and Theories in Biotechnology - NATO ARW Proceedings*, Juan Bertran, Ed., Kluwer Academic Publishers, 1992

Reaction Dynamics in Polyatomic Molecular Systems: Some Approaches for Constructing Potential Energy Surfaces and Incorporating Quantum Effects in Classical Trajectory Simulations

W.H. Miller

October 1991

Prepared for the U.S. Department of Energy under Contract Number DE-AC03-76SF00098

DISCLAIMER

LBL-31626

Reaction Dynamics in Polyatomic Molecular Systems: Some Approaches for Constructing Potential Energy Surfaces and Incorporating Quantum Effects in Classical Trajectory Simulations

William H. Miller

Department of Chemistry
University of California

and

Chemical Sciences Division
Lawrence Berkeley Laboratory
University of California
Berkeley, California 94720

October 1991

This work was supported by the Director, Office of Energy Research, Office of Basic Energy Sciences, Chemical Sciences Division, of the U.S. Department of Energy under Contract No. DE-AC03-76SF00098.

REACTION DYNAMICS IN POLYATOMIC MOLECULAR SYSTEMS: SOME APPROACHES FOR CONSTRUCTING POTENTIAL ENERGY SURFACES AND INCORPORATING QUANTUM EFFECTS IN CLASSICAL TRAJECTORY SIMULATIONS

WILLIAM H. MILLER
Department of Chemistry, University of California, and
Chemical Sciences Division of the Lawrence Berkeley Laboratory,
Berkeley, California 94720

ABSTRACT. This paper deals with the two essential tasks necessary to model chemical reactions theoretically: obtaining the potential energy surface (i.e., the electronic energy of the molecular system as a function of nuclear positions) and then determining the dynamical motion of the nuclei/atoms governed by it.

It is sometimes possible to model the potential energy surface for a chemical reaction *locally*, e.g., a harmonic valley along the *reaction path* which passes through the transition state (saddle point on the potential energy surface) connecting reactants and products. More generally, though, it is necessary to have a *global* potential energy function that is not restricted to the vicinity of reaction path. Many completely empirical potential functions have been developed for non-reactive molecular motions, and it is shown here how the *empirical valence bond* (EVB) idea can be used to combine these non-reactive potential functions, which describe reactant and product regions individually, with *ab initio* calculations for the transition state region and thus obtain a global potential energy surface for a chemical reaction.

Although the dynamics of nuclear motion should in principle be treated quantum mechanically, the difficulty of doing so is prohibitive for polyatomic systems. Most dynamical treatments employ classical mechanics which, though an excellent approximation in many regards, has some serious deficiencies. One such problem discussed here has to do with zero point vibrational energy and the other with tunneling of light (e.g., hydrogen) atoms. Though quite rigorous semiclassical theories exist that would in principle solve these problems, we describe in this paper more approximate approaches that are intended to be suitable for direct incorporation into classical simulation algorithms.

1. Introduction

This lecture will not deal explicitly with biological applications, but rather will describe some recent developments in theoretical/computational methodology that could have practical implications for dynamical simulations of such processes. All of the theoretical approaches discussed here are "trajectory based", i.e., geared to be utilized within the framework of a classical trajectory simulation of the atomic/molecular motion. Though the applications carried out in my research group are for medium size polyatomic molecules — e.g., the intramolecular isomerization in malonaldehyde,

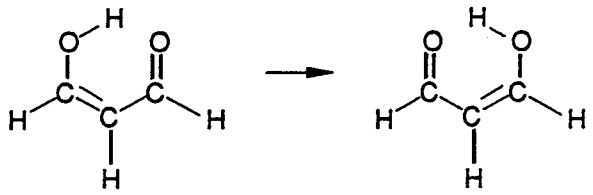

(1. 1)

1 2

— I believe that the issues involved, and the methodologies being developed, also have relevance for the more complex molecular systems of biological interest.

The following three sections deal with three separate issues involving classical trajectory simulations in polyatomic systems: (1) convenient (and accurate!) representations of a global potential energy surface for *reactive* systems; (2) how to deal with the problem of zero point (vibrational) energy in polyatomic molecules; and (3) how to incorporate tunneling (primarily in H atom transfer reactions) into trajectory simulations in an accurate, yet practically manageable way.

2. An Empirical Valence Bond Model for Reactive Potential Energy Surfaces

One of the most difficult steps in theoretical treatments of chemical reactions in polyatomic molecular systems is representing the potential energy surface.[1] Ideally, of course, one would like to be able to compute the Born-Oppenheimer electronic energy $V(q_1,...,q_{3N-6})$ from first principles for any values of the 3N-6 coordinates that are necessary to specify the configuration of the N atom system. Though *ab initio* quantum chemistry calculations[2] are becoming increasingly possible for polyatomic molecular

systems, the number of such calculations needed for more than 3 or 4 atom systems tends to make this direct approach unfeasible.

One of the ways used for dealing with the situation has been to exploit the idea of a reaction path.[3-5] Here one computes the potential energy surface only along a one-dimensional curve (the reaction path) in the 3N-6 dimensional space that connects reactant and product configurations. This is often the steepest descent path (in mass-weighted cartesian coordinates) that passes through the transition state for the reaction under study — the "intrinsic" reaction path[5] — but other paths are possible[6] and sometimes more useful.[7] One typically also determines the force constant matrix along this path, thus providing a local harmonic approximation to the potential energy surface along the reaction (or reference) path.

Though reaction path approaches have been very useful, particularly for qualitative and approximate dynamical treatments, and will certainly continue to be so, there are times when a global potential energy surface is needed. This is true, for example, for highly vibrationally excited molecules, where the dynamics tends not to be localized about any one reaction path, and also for cases with a number of low frequencies modes orthogonal to the reaction path, which allows for large amplitude motion far away from any reference path.

For vibrational motions about stable molecular geometries a standard normal mode expansion — harmonic plus perhaps anharmonic corrections — provides an adequate global potential function. There also exist a number of completely empirical potential functions[8-12] that describe a variety of non-reactive motions and interactions. Unless special alterations are made, however, these potential functions are not capable of modeling the potential energy surface for a chemical reaction.

In this paper we wish to pursue and develop an approach used by Warshel[13] that is especially designed to model reactive potential functions, namely the empirical valence bond (EVB) model. To illustrate the basic idea, consider an isomerization reaction such as Eq. (1.1), which is characterized by a multi-dimensional double well potential function. One *imagines* that this Born-Oppenheimer potential energy surface results from a quantum chemistry calculation with a 2-state valence bond electronic wavefunction

$$|\psi\rangle = c_1|\phi_1\rangle + c_2|\phi_2\rangle, \tag{2.1}$$

where $|\phi_1\rangle$ is a valence bond wavefunction that describes the electronic structure of the

reactants (1) in Eq. (1.1), and $|\phi_2\rangle$ the corresponding wavefunction that describes the electronic structure of the products (2). The lowest electronic eigenvalue, i.e., the Born-Oppenheimer potential energy surface, is then given by the lower root of the 2x2 secular equation, specifically

$$V = 1/2\,(V_{11}+V_{22}) - \sqrt{\left(\frac{V_{11}-V_{22}}{2}\right)^2 + V_{12}^2}\,, \tag{2.2}$$

where

$$V_{11} = \langle\phi_1|H_{el}|\phi_1\rangle$$

$$V_{22} = \langle\phi_2|H_{el}|\phi_2\rangle$$

$$V_{12} = \langle\phi_1|H_{el}|\phi_2\rangle\,,$$

and H_{el} is the electronic Hamiltonian. V is a function of the nuclear coordinates $\mathbf{q} \equiv (q_1, ..., q_{3N-6})$ because the electronic Hamiltonian depends on $\mathbf{q}$, and thus V_{11}, V_{22}, and V_{12} also do.

In the *empirical* valence bond approach, however, no electronic matrix elements are actually calculated. $V_{11} \equiv V_{11}(q_1, ..., q_{3N-6})$ is identified as the potential energy surface for the reactants and thus taken as a non-reactive (i.e., single minimum) potential energy surface that describes non-reactive motion about the reactant geometry. The simplest imaginable model for $V_{11}(\mathbf{q})$ would be a harmonic normal mode approximation about the reactant equilibrium geometry. At a more sophisticated level, one could use one of the non-reactive empirical potential models[8-12] that has the bonding designated as in (1) of Eq. (1.1). $V_{22}(\mathbf{q})$ is similarly a non-reactive (i.e., single minimum) potential energy surface that describes motion about the product geometry. V_{11} and V_{22} are often referred to as *diabatic* potential surfaces, in contrast to V itself which is the Born-Oppenheimer, or *adiabatic* potential surface.

The most crucial part of the EVB model is the exchange matrix element (or resonance integral) $V_{12} = V_{12}(\mathbf{q})$, for it is less obvious how it should be chosen. Warshel[13] has used some very simple approximations in his (very complex) applications, while here we describe a way of choosing it so that the EVB potential $V(\mathbf{q})$ of Eq. (2.2)

exactly reproduces a given harmonic force field about a given transition state geometry. We envision that the transition state quantities (geometry, energy, and force constant matrix) will be obtained by *ab initio* quantum chemistry calculations. I.e., the logic of the approach is that *ab initio* quantum calculations of useful accuracy can be carried out for a few selected features of the reactive potential surface, and the most important of these are the transition state parameters since this is the least well known region of the potential and also the most important region for describing the reaction. The reactant and product regions are described reasonably well by simple (non-reactive) empirical potential functions[8-12] for stable molecules. The EVB model that we present is thus a way of incorporating *ab initio* calculations for the transition state parameters with simple diabatic potential functions that describe reactants and products separately.

The potential energy surface $V(\mathbf{q})$ is thus taken to be in the form of Eq. (2.2), where the diabatic potentials $V_{11}(\mathbf{q})$ and $V_{22}(\mathbf{q})$ are non-reactive (i.e., single minimum) potential functions that correctly describe the regions near the equilibrium geometries $\mathbf{q}_1$ and $\mathbf{q}_2$, respectively. V_{11} and V_{22} are assumed to be known, and the goal is to find a useful way of determining the exchange matrix element $V_{12}(\mathbf{q})$. It is clear that in the reactant or product regions themselves, i.e., for $\mathbf{q}$ near $\mathbf{q}_1$ or $\mathbf{q}_2$, one will have

$$V_{12}^2 \ll \left(\frac{V_{11}-V_{22}}{2}\right)^2 , \tag{2.3a}$$

and in this limit it is easy to see that Eq. (2.2) gives

$$V(\mathbf{q}) \cong \mathrm{Min}[V_{11}(\mathbf{q}),V_{22}(\mathbf{q})], \tag{2.3b}$$

which is clearly correct in these regions. It is thus only necessary to know $V_{12}(\mathbf{q})$ in the intermediate region between reactants and products, and to determine it in this region we appeal to *ab initio* quantum chemistry.

Eq. (2.2) can be used to express V_{12} in terms of V_{11}, V_{22}, and V as follows,

$$V_{12}(\mathbf{q})^2 = [V_{11}(\mathbf{q})-V(\mathbf{q})][V_{22}(\mathbf{q})-V(\mathbf{q})]. \tag{2.4}$$

Near the transition state geometry one has

$$V(\mathbf{q}) \cong V_0 + 1/2\ (\mathbf{q}-\mathbf{q}_0)\bullet\mathbf{K}_0\bullet(\mathbf{q}-\mathbf{q}_0), \tag{2.5}$$

where the transition state geometry $\mathbf{q}_0$, energy V_0, and force constant matrix $\mathbf{K}_0$ are obtained from an independent *ab initio* calculation. Since the non-reactive potential functions $V_{11}(\mathbf{q})$ and $V_{22}(\mathbf{q})$ are known, they can also be expanded in a Taylor's series about the transition state geometry

$$V_{nn}(\mathbf{q}) = V_n + \mathbf{D}_n\bullet\Delta\mathbf{q} + 1/2\ \Delta\mathbf{q}\bullet\mathbf{K}_n\bullet\Delta\mathbf{q}\ , \tag{2.6}$$

where $\Delta\mathbf{q} = \mathbf{q}-\mathbf{q}_0$,

$$V_n = V_{nn}(\mathbf{q}_0)\ ,$$

$$\mathbf{D}_n = \left(\frac{\partial V_{nn}(\mathbf{q})}{\partial \mathbf{q}}\right)_{\mathbf{q}=\mathbf{q}_0}$$

$$\mathbf{K}_n = \left(\frac{\partial^2 V_{nn}(\mathbf{q})}{\partial \mathbf{q}\partial \mathbf{q}}\right)_{\mathbf{q}=\mathbf{q}_0}$$

for n=1,2. With Eqs. (2.5) and (2.6), Eq. (2.4) thus gives the following power series expansion for V_{12}^2, correct through quadratic order in $\Delta\mathbf{q}\equiv\mathbf{q}-\mathbf{q}_0$,

$$\begin{aligned} V_{12}^2 = {} & (V_1-V_0)(V_2-V_0) + (V_2-V_0)\ \mathbf{D}_1\bullet\Delta\mathbf{q} + (V_1-V_0)\ \mathbf{D}_2\bullet\Delta\mathbf{q} \\ & + 1/2\ (V_1-V_0)\Delta\mathbf{q}\bullet(\mathbf{K}_2-\mathbf{K}_0)\bullet\Delta\mathbf{q} + 1/2\ (V_2-V_0)\Delta\mathbf{q}\bullet(\mathbf{K}_1-\mathbf{K}_0)\bullet\Delta\mathbf{q} \\ & + (\mathbf{D}_1\bullet\Delta\mathbf{q})(\mathbf{D}_2\bullet\Delta\mathbf{q}). \end{aligned} \tag{2.7}$$

A cumulant resummation,[14] though, gives better extrapolation properties; therefore $V_{12}^2(\mathbf{q})$ is taken to be a generalized Gaussian

$$V_{12}^2(\mathbf{q}) = A\ \exp\ [\mathbf{B}\bullet\Delta\mathbf{q}-1/2\ \Delta\mathbf{q}\bullet\mathbf{C}\bullet\Delta\mathbf{q}]\ , \tag{2.8}$$

and this function expanded through quadratic order in $\Delta\mathbf{q}$ and equated to the

corresponding terms on the RHS of Eq. (2.7) to determine the parameters A, **B** (a vector) and **C** (a matrix). The arithmetic is straight-forward and one obtains

$$A = (V_1-V_0)(V_2-V_0) \tag{2.9a}$$

$$\mathbf{B} = \frac{\mathbf{D}_1}{(V_1-V_0)} + \frac{\mathbf{D}_2}{(V_2-V_0)} \tag{2.9b}$$

$$\mathbf{C} = \frac{\bullet\mathbf{D}_2\mathbf{D}_2\bullet}{(V_2-V_0)^2} + \frac{\bullet\mathbf{D}_1\mathbf{D}_1\bullet}{(V_1-V_0)^2} + \frac{(\mathbf{K}_0-\mathbf{K}_1)}{V_1-V_0} + \frac{(\mathbf{K}_0-\mathbf{K}_2)}{V_2-V_0} . \tag{2.9c}$$

For completeness, we note that if the intermediate position $\mathbf{q}_0$ is actually not the transition state geometry, so that Eq. (2.5) has a linear term $\mathbf{D}_0\bullet\Delta\mathbf{q}$, then Eqs. (2.7)-(2.9) still apply if the following change is made in (2.9b) and (2.9c),

$$\mathbf{D}_n \rightarrow \mathbf{D}_n-\mathbf{D}_0 , \tag{2.9d}$$

for n=1,2.

Eqs. (2.8)-(2.9) are the basic theoretical content of the model. They give a very simple prescription for the exchange matrix element that will cause the EVB potential Eq. (2.2) to reproduce a given harmonic force field about a given transition state (or any other intermediate) geometry. Because of its Gaussian form, V_{12} is damped out away from this region so that the EVB expression [Eq. (2.2)] reduces to V_{11} or V_{22} in the reactant and product regions. It thus provides a useful way to incorporate *ab initio* quantum chemistry calculations for the transition state with simple empirical potential functions which model the non-reactive motions of the reactants and products.

We now apply this version of the EVB model to some simple, but non-trivial, test problems to illustrate its capabilities (and limitations) in a variety of situations. The first example is a two-dimensional double well potential function that has been used previously[15] as a test of various dynamical theories and also as a model for isomerization reactions such as Eq. (1.1). The specific form of the potential function is

$$V(s,Q) = V_0(s) + 1/2\, m\omega^2 \left(Q - \frac{cs^n}{m\omega^2}\right)^2, \tag{2.10}$$

where $V_0(s)$ is a one-dimensional symmetric double well potential, and c is a coupling constant which characterizes the strength of the coupling between the "reaction coordinate" s and the "bath mode" Q. Written in this re-normalized form, the barrier height is independent of the coupling constant. n=1 or 2 in Eq. (2.10) determines the symmetry of the coupling. In all cases the mass m is that of a hydrogen atom and the one-dimensional double well potential is

$$V_0(s) = 1/2\ (v_{11}(s) + v_{22}(s)) - \sqrt{\left(\frac{v_{11}(s)-v_{22}(s)}{2}\right)^2 + v_{12}(s)^2} \qquad (2.11a)$$

where

$$v_{11}(s) = 1/2\ \ m\omega_0^2(s+s_0)^2 \qquad (2.11b)$$

$$v_{22}(s) = 1/2\ \ m\omega_0^2(s-s_0)^2 \qquad (2.11c)$$

$$v_{12}(s) = a\ \exp(-bs^2)\ , \qquad (2.11d)$$

with parameters ω_0 = 1600 cm-1, s_0 = 1, a = 0.036065963, b = 1.781678095 (all distances in atomic units). These parameters yield a barrier height of ~8.2 kcal/mole, which is typical of H atom transfer.

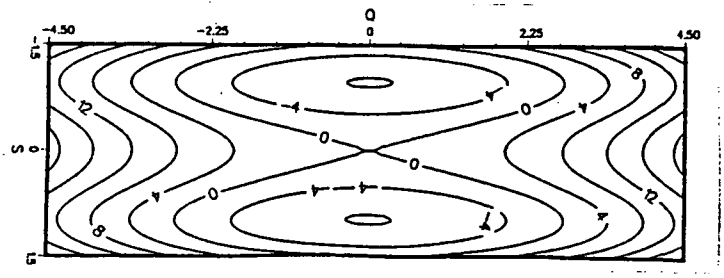

Figure 1. The double well potential energy surface of Eq. (2.10), for the uncoupled case (c=0) and a low frequency (ω=300 cm^{-1}) bath mode Q. The coordinates are in atomic units and the contour values in kcal/mole.

The examples below consider the case of a low frequency (ω = 300 cm^{-1}) or a high frequency (ω = 3000 cm^{-1}) bath mode, and in all cases here the diabatic potentials V_{11}

and V_{22} are taken as the harmonic normal mode potentials for reactants and products; i.e.,

$$V_{11}(s,Q) = 1/2\ m\omega_1^2\ s'^2 + 1/2\ m\omega_2^2\ Q'^2 \tag{2.12a}$$

$$V_{22}(s,Q) = 1/2\ m\omega_1^2\ s''^2 + 1/2\ m\omega_2^2\ Q''^2 \tag{2.12b}$$

where s' and Q' are the normal mode coordinates (linear combinations of s and Q) about the reactant minimum on the potential surface, and s" and Q" are the product normal mode coordinates. (The normal mode frequencies ω_1 and ω_2 are the same for reactants and products in this example because of symmetry.) As discussed in the Introduction, this is the simplest possible choice for the diabatic potentials.

Figure 1 shows a contour plot of the uncoupled (c=0) potential surface, Eq. (2.10)-(2.11), for the case of a low frequency ($\omega \equiv 300\ cm^{-1}$) bath mode. Since the one-dimensional double well function $V_0(s)$ of Eq. (2.11) is of EVB form, it is clear the general EVB model, Eq. (2.2) and (2.8)-(2.9), will exactly reproduce the potential in the uncoupled limit. It is thus of interest to see how the EVB model performs as the coupling c is increased.

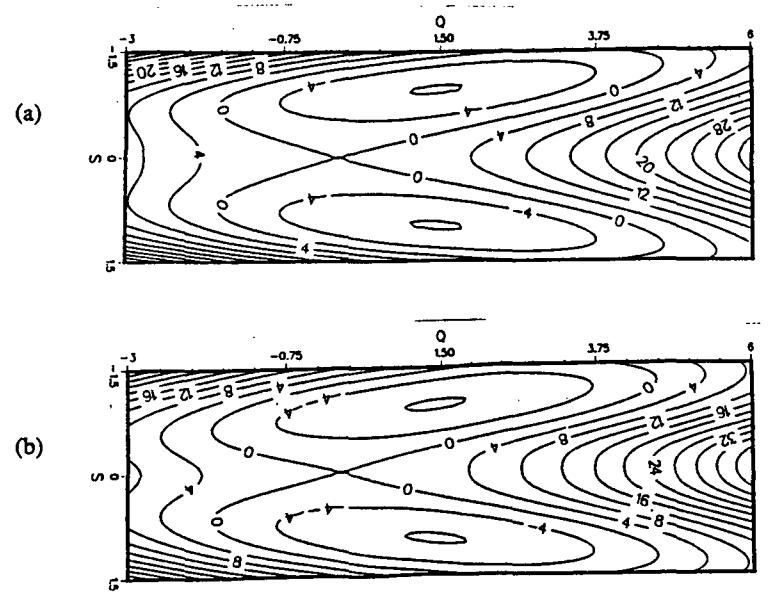

Figure 2. Same as Fig. 1, but for even (n=2) coupling with the constant c=0.005. (a) The original potential of Eq. (2.10). (b) The EVB approximation given by Eqs. (2.2) and (2.8)-(2.9), with the harmonic diabatic potentials of Eq. (2.12).

Figures 2a and 2b show contour plots of the original potential and the EVB approximation to it, respectively, for a modest size even (n=2 in Eq. (2.10)) coupling constant. Though some quantitative differences are apparent, on the whole the EVB model does an excellent job in representing the important regions of the potential energy surface.

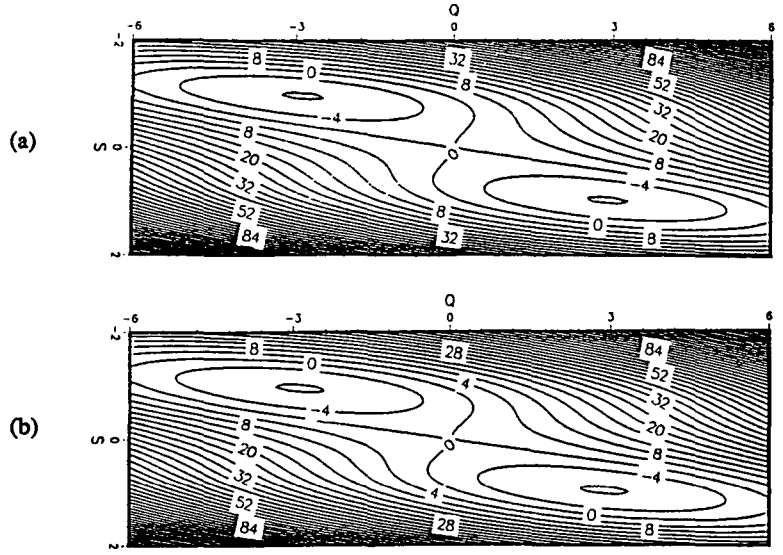

Figure 3. Same as Fig. 1, but for odd (n=1) coupling with the constant c=0.01. (a) The original potential. (b) The EVB approximation (with harmonic diabatic potentials).

Figures 3a and 3b show a similar comparison for the case of odd (n=1 in Eq. (2.10)) coupling. (This example is very close to a two-dimensional model relevant to double H atom transfer in formic acid dimer.) Though the coupling causes a dramatic change in the potential surface from the uncoupled case in Figure 1, one sees that EVB model again provides an excellent description of this potential surface.

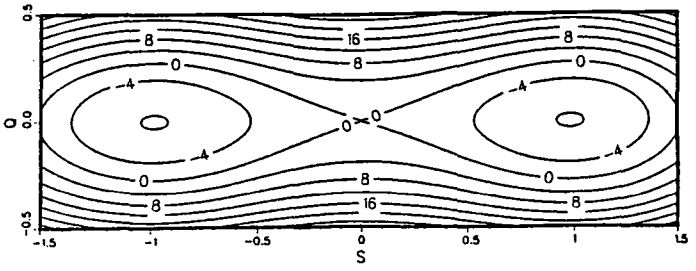

Figure 4. The double well potential function of Eq. (2.10), for the uncoupled case (c=0) and a high frequency (ω=3000 cm^{-1}) bath mode Q.

High frequency bath modes are usually easier to describe correctly than low frequency ones because the steeper harmonic potential does not allow for as large excursions in such degrees of freedom. Figure 4 shows the uncoupled (c=0) double well potential function of Eq. (2.10) for the case of a high frequency ($\omega = 3000\ cm^{-1}$) bath mode. Again, the EVB model exactly reproduces the potential in the uncoupled limit, so we consider its behavior for non-zero coupling.

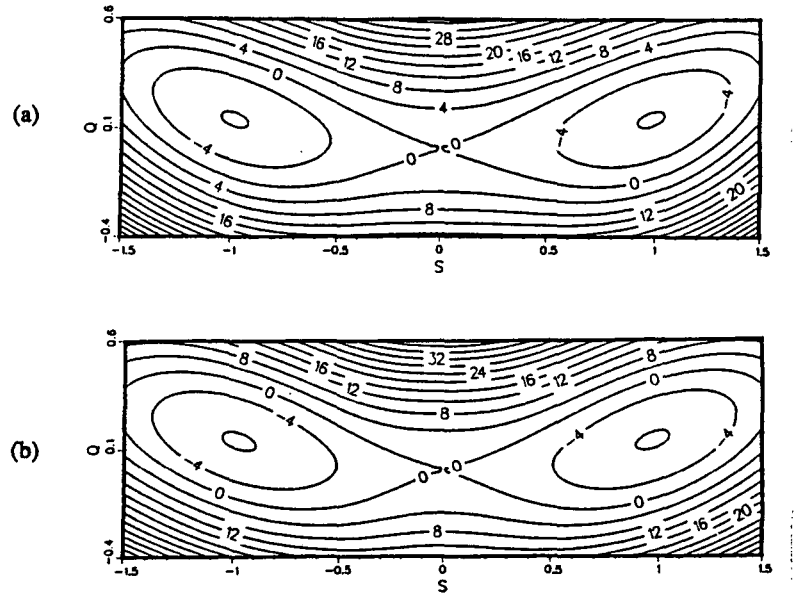

Figure 5. Same as Fig. 4, but for even coupling with the constant c=0.05. (a) The original potential. (b) The EVB approximation (with harmonic diabatic potentials).

Figures 5a and 5b show the original potential and its EVB approximation, respectively, for the case of even coupling, and Figures 6a and 6b show a similar comparison for odd coupling, both for fairly large coupling constants. (The potential wells are displaced less drastically from their uncoupled position than for the low frequency case because the high frequency of the bath mode makes the potential "stiffer" with regards to perturbation in the Q-direction.) In both cases one sees that the EVB model provides an excellent description of the true potential.

These examples show that the EVB model, with the exchange potential V_{12} chosen to reproduce the transition state region of the potential energy surface, is able to provide an excellent global description of reactive potential surfaces for a wide variety of situations. These examples have all used the simplest possible choice for the diabatic

potential V_{11} and V_{22}, namely a harmonic normal model approximation about their respective minima. One can improve the model by using more accurate diabatic potentials, ones that represent the true potential more accurately over wider regions, for in this case the exchange potential is required to describe matters in a smaller region about the transition state.

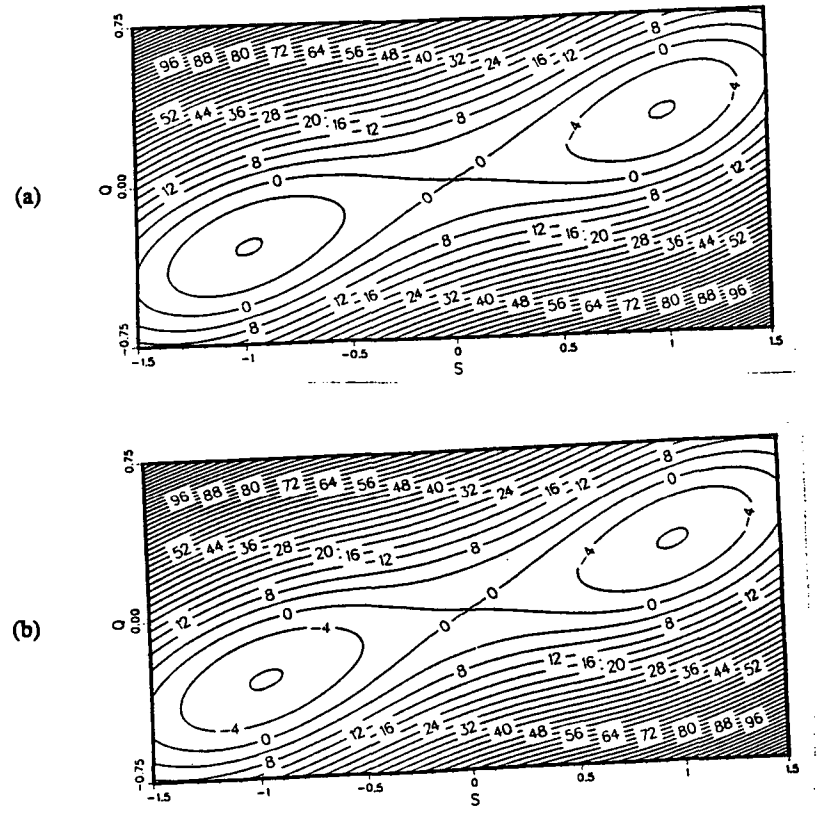

Figure 6. Same as Fig. 4, but for odd coupling with the constant c=0.1. (a) The original potential. (b) The EVB approximation (with harmonic diabatic potentials).

3. How to Deal with the Zero Point Energy Problem in Classical Mechanics

One of the frustrating shortcomings in using classical mechanics to simulate dynamical processes in polyatomic molecules has to do with a problem involving the zero point energy of vibrational degrees of freedom.[16-18] To describe the problem, recall first the

simpler situation of an atom-diatom (gas phase) bimolecular reaction,

$$A + BC(v_i=0) \rightarrow AB(v_f) + C, \qquad (3.1)$$

where it is indicated that the reactant diatom BC is initially in its ground vibrational state. It is well-known that a classical trajectory simulation[19] of this process works best if initial conditions for the trajectories are chosen to have the correct zero point vibrational energy in the diatom, with the initial phase of the vibrational motion selected at random (i.e., averaged over), so-called "quasiclassical" initial conditions. Agreement with (the correct) quantum reaction probabilities, or cross sections, would be much worse if the trajectory were begun with *no* vibrational energy. A problem can arise even for this simple process if the reaction is endoergic and most of the product is produced in v_f=0. It is possible classically to obtain reactive trajectories with less than the zero point vibrational energy in the product molecule AB, clearly an unphysical result since this permits reaction below the quantum threshold for the reaction! This problem is usually dealt with[20] by performing the classical simulation always in the *exoergic* direction and then using microscopic reversibility to obtain probabilities or cross sections in the reverse direction.

One thus believes that a classical simulation of a *polyatomic* molecular system will mimic nature (i.e., quantum mechanics) more closely if trajectories are begun with (at least) zero point vibrational energy in all vibrational degrees of freedom, with the phases of the vibrational motion selected at random (i.e., averaged over). To simulate vibrational relaxation of CH local mode overtones in benzene,[21,22] for example, it would seem most reasonable to begin trajectories with the appropriate vibrational energy in the CH stretch and zero point vibrational energy in all the other normal modes.

Since the potential energy function for the polyatomic system is in general anharmonic, energy can flow between various degrees of freedom; often, in fact, it is this intramolecular vibrational energy redistribution (IVR) that one is wishing to simulate. The "zero point energy problem"[16-18] mentioned in the first paragraph is that the energy in some vibrational modes may fall below the (quantum) zero point energy ($1/2\hbar\omega_k$, where ω_k is the harmonic frequency for mode k). This may not at first seem like a serious problem, but in even a medium size polyatomic molecule (e.g., benzene) the zero point energy is a sizeable amount of energy (52.2 kcal/mole in benzene). It is a particularly serious problem if the zero point energy flows out of several modes and

"pools" into a specific weak bond. For large molecules it may even happen that the classical mechanics is chaotic at its zero point energy. These are all clearly unphysical effects that arise because classical mechanics cannot prevent the energy in each vibrational mode from dipping below its zero point value.

Here we describe a model for modifying the classical equations of motion in order to remedy this situation, i.e., to prevent the vibrational energy in each mode from at any time dipping below its zero point value. The algorithm we present affects the classical trajectory only when the vibrational energy of a mode attempts to decrease below its zero point value; otherwise the trajectory is the ordinary classical one. The algorithm conserves the total energy of the polyatomic system, and since it prevents the energy in each mode from decreasing below its zero point value, there can be no unphysical "energy pooling" of the zero point energy from many modes into one bond.

The model is first described in its simplest version, and then a more general version. The resulting algorithm is actually quite simple: if the energy in any mode k, say, decreases below its zero point value at time t, then at this time the (Cartesian) momentum p_k has its sign changed, and the trajectory continues; this is essentially a *time reversal* for mode k (only!). One can think of the model as supplying impulsive "quantum kicks" to a mode whose energy is trying to fall below its zero point value, i.e., a kind of "Planck demon" analogous to a Brownian-like random force.

The Hamiltonian is assumed to be of standard Cartesian form

$$H(\mathbf{p},\mathbf{x}) = 1/2\ \mathbf{p}^2 + V(\mathbf{x}), \tag{3.2}$$

where $\mathbf{x}\equiv\{x_k\}$ are the mass-weighted Cartesian coordinates of the system. The potential energy function consists of a harmonic part plus an anharmonic coupling,

$$V(\mathbf{x}) = V_0(\mathbf{x}) + V_1(\mathbf{x}) \tag{3.3a}$$

where

$$V_0(x) = \sum_k 1/2\ \omega_k^2 x_k^2 \tag{3.3b}$$

It is useful to introduce the usual harmonic action-angle variables (n_k,q_k), in terms of which the Cartesian variables are

$$\chi_k = \sqrt{(2n_k+1)\hbar/\omega_k}\,\cos q_k \tag{3.4a}$$

$$p_k = -\sqrt{(2n_k+1)\hbar\omega_k}\,\sin q_k \tag{3.4b}$$

In terms of the action-angle variables, the Hamiltonian is

$$H(\mathbf{n},\mathbf{q}) = H_0(\mathbf{n}) + V_1[(\mathbf{x}(\mathbf{n},\mathbf{q})], \tag{3.5a}$$

where

$$H_0(\mathbf{n}) = \sum_k \hbar\omega_k\,(n_k+1/2). \tag{3.5b}$$

The actions $\{n_k\}$ are the classical counterparts to the harmonic quantum numbers, and the angles $\{q_k\}$ are the phases of the vibrational motion. [The actions $\{n_k\}$ are actually the classical action in units of $\hbar$, with the added constant "1/2" so that integer values of $\{n_k\}$ correspond to the quantum numbers; i.e., n_k = (classical action)/$\hbar$ - 1/2.]

We seek a modified classical mechanics that maintains

$$n_k(t)\geq 0 \tag{3.6}$$

at all times and for all modes k. This is accomplished by adding to the Hamiltonian hard wall terms $W(n_k)$, such that

$$W(n_k) = \begin{cases} 0, & n_k>0 \\ +\infty, & n_k<0 \end{cases}. \tag{3.7}$$

This is analogous to a hard sphere repulsive potential V(r) that keeps an interparticle distance r(t) greater than a hard sphere radius r(t), i.e.,

$$V(r) = \begin{cases} 0, & r>r_0 \\ +\infty, & r<r_0 \end{cases} \tag{3.8}$$

In the hard sphere case it is well-known how to deal with the situation: the hard sphere potential (3.8) has no effect unless r(t) decreases to the value r_0, at which time one makes the instantaneous change

$$\begin{pmatrix} r(t) \\ p_r(t) \end{pmatrix} \rightarrow \begin{pmatrix} r(t) \\ -p_r(t) \end{pmatrix} \tag{3.9}$$

i.e., the hard spheres experience an impulsive collision and are reflected. We follow this same course for the hard wall term in the action variable, Eq. (3.7).

Thus the hard wall potentials of Eq. (3.7) have no effect so long as $n_k(t) \geq 0$, but if $n_k(t)$ dips below zero at some time along the trajectory, one makes the replacement

$$\begin{pmatrix} n_k(t) \\ q_k(t) \end{pmatrix} \rightarrow \begin{pmatrix} n_k(t) \\ -q_k(t) \end{pmatrix} \tag{3.10}$$

Eq. (3.10) results from integrating the classical equations of motion with the hard wall potential $W(n_k)$ over the infinitesimal time increment of the impulsive interaction. By using Eq. (3.4), this can be expressed in terms of the original Cartesian variables as

$$\begin{pmatrix} x_k(t) \\ p_k(t) \end{pmatrix} \rightarrow \begin{pmatrix} x_k(t) \\ -p_k(t) \end{pmatrix} \tag{3.11}$$

Eq. (3.11) shows that the modification made to mode k at time t is essentially a *time reversal* for that mode. Only the mode for which $n_k(t)$ dips below 0 is modified as in (3.11).

One can verify more directly that (3.11) will indeed keep $n_k(t) > 0$. Hamilton's equations show that

$$\frac{d}{dt}\hbar n_k(t) = -\frac{\partial H(\mathbf{n},\mathbf{q})}{\partial q_k} = -\frac{\partial V_1}{\partial q_k}$$

$$= -\frac{\partial V_1}{\partial x_k}\frac{\partial x_k}{\partial q_k}$$

$$= -\frac{\partial V_1}{\partial x_k} p_k/\omega_k. \qquad (3.12)$$

Thus if $n_k(t)$ is decreasing through 0 at time t_0 — i.e., $n_k(t_0) = 0$ and $\dot{n}_k(t_0) < 0$ — making the replacement $p_k \rightarrow -p_k$ will change the sign of $\dot{n}_k$ [cf. Eq. (3.12)] so that $\dot{n}_k(t_0) > 0$, and $n_k(t)$ will then increase and remain above 0. Since the Hamiltonian (3.2) is Cartesian, it is also clear that the instantaneous modification (3.11) conserves the value of H, i.e., the total energy.

The algorithm may be summarized as follows, all in terms of the original Cartesian variables:

1) Start the trajectory in the appropriate manner (e.g., quasiclassical initial conditions).

2) At the end of each time step in the trajectory, insert the Fortran statement

$$p_k = p_k * \text{Sign}\,(1/2\, p_k^2 + 1/2\omega_k^2 x_k^2 - 1/2\hbar\omega_k) \qquad (3.13)$$

for all k.

3) Keep on computing!

Eq. (3.13) clearly accomplishes the modifications discussed above.

The simple version of the model described above prevents the zeroth order actions $\{n_k(t)\}$ of the fixed-frequency reference Hamiltonian H_0, Eq. (3.5), from becoming negative. If the dynamics of interest involves motion about a relatively well-defined equilibrium geometry, then this treatment may be adequate. In the more extreme case of a fragmentation process, e.g., unimolecular decomposition, however, it will not be a reasonable description because the physically relevant modes of the system change radically (the frequencies of some vibrations even going to zero as they evolve into

rotations). In this section we show how the simple model above can be generalized by applying it to the zero point energy of the *instantaneous* normal modes.

Thus at every time t along the classical trajectory $\mathbf{x}(t)$ we determine the energy in the various instantaneous normal modes, and then require that this not be below their respective zero point values. At the arbitrary time t, therefore, the potential is expanded through quadratic terms about the instantaneous position $\mathbf{x}(t)\equiv\mathbf{x}_t$,

$$\mathbf{V}(\mathbf{x}) \equiv \mathbf{V}(\mathbf{x}_t) + \mathbf{f}(\mathbf{x}_t)^T \cdot (\mathbf{x}-\mathbf{x}_t) + 1/2(\mathbf{x}-\mathbf{x}_t)^T \cdot \mathbf{K}(\mathbf{x}_t) \cdot (\mathbf{x}-\mathbf{x}_t), \tag{3.14a}$$

where

$$\mathbf{f}(\mathbf{x}) = \frac{\partial \mathbf{V}(\mathbf{x})}{\partial \mathbf{x}} \tag{3.14b}$$

$$\mathbf{K}(\mathbf{x}) = \frac{\partial^2 \mathbf{V}(\mathbf{x})}{\partial \mathbf{x}\partial \mathbf{x}} \tag{3.14c}$$

If $\{\mathbf{L}_k\}$ are the eigenvectors of the force constant matrix $\mathbf{K}(\mathbf{x}_t)$ and Ω_k^2 the eigenvalues, then the local normal coordinates $\mathbf{Q}$ and momenta $\mathbf{P}$ are related to the original Cartesian variables $(\mathbf{x},\mathbf{p})$ by

$$\mathbf{x} - \mathbf{x}_t \equiv \sum_k \mathbf{L}_k Q_k = \mathbf{L}\cdot\mathbf{Q}, \tag{3.15a}$$

$$\mathbf{p} = \mathbf{L}\cdot\mathbf{P} \tag{3.15b}$$

Within this local quadratic approximation about $\mathbf{x}_t$, the Hamiltonian is given in terms of the local normal mode variables $(\mathbf{Q},\mathbf{P})$ by

$$\mathbf{H}(\mathbf{P},\mathbf{Q}) \equiv \mathbf{V}(\mathbf{x}_t) + \sum_k (1/2P_k^2 + D_k Q_k + 1/2\Omega_k^2 Q_k^2), \tag{3.16a}$$

where $\{D_k\} \equiv \mathbf{D}$ is given by

$$\mathbf{D} = \mathbf{L}^T \cdot \mathbf{f}(\mathbf{x}_t). \tag{3.16b}$$

Eq. (3.16a) is a sum of one-dimensional harmonic oscillator Hamiltonians, each with a shifted equilibrium position,

$$1/2P_k^2 + D_kQ_k + 1/2\Omega_k^2Q_k^2 = 1/2P_k^2 + 1/2\Omega_k^2[Q_k+(D_k/\Omega_k^2)]^2 - (D_k^2/2\Omega_k^2), \tag{3.17a}$$

so that the zero point energy constraint is

$$1/2P_k^2+ D_kQ_k + 1/2\Omega_k^2Q_k^2 \geq 1/2\hbar\Omega_k - (D_k^2/2\Omega_k^2), \tag{3.17b}$$

for each mode k. We are actually interested in imposing this constraint at the instantaneous position $\mathbf{x} = \mathbf{x}_t$, i.e., $\mathbf{Q} = 0$, so that the constraints we wish to impose are

$$1/2P_k^2 + (D_k^2/2\Omega_k^2) \geq 1/2\hbar\Omega_k \tag{3.18a}$$

for all k. In terms of the original Cartesian coordinates and momenta, this reads

$$1/2(\mathbf{L}_k^T\bullet\mathbf{p})^2 + 1/2(\mathbf{L}_k^T\bullet\frac{\partial V}{\partial \mathbf{x}})^2/\Omega_k^2 \geq 1/2\hbar\Omega_k. \tag{3.18b}$$

The left hand side of Eq. (3.18) may be thought of as the instantaneous (i.e., at time t) energy in the local, harmonic mode k: the first term of (3.18b) is clearly the kinetic energy in mode k, and the second term is the potential energy which is due to the fact that the position $\mathbf{x}(t)$ is not at the minimum of the instantaneous harmonic potential. If some of the frequencies Ω_k are zero, or imaginary (i.e., mode k corresponds to moving over a barrier rather than in a well), then one does not apply a zero point energy constraint because there is no quantum zero point energy for such modes. We note also that more rigorously, one should diagonalize the *projected force constant matrix*,[4a] so that the six degrees of freedom corresponding to overall translations and rotations of the polyatomic system will yield zero frequencies and thus have no zero point energy constraint.

We thus summarize, in terms of the original Cartesian variables, the more general algorithm as follows:

1. Begin the trajectory in the appropriate manner to describe the process of interest.
2. After each time step diagonalize the force constant matrix $\partial^2V/\partial\mathbf{x}\partial\mathbf{x}$ (more

rigorously, the *projected* force constant matrix) at the current position x(t), yielding the eigenvalues Ω_k^2 and eigenvectors $\{\mathbf{L}_k\}$.

3. For all modes k for which $\Omega_k^2>0$, make the replacement

$$\mathbf{p} \rightarrow \mathbf{p} - 2\mathbf{L}_k(\mathbf{L}_k^T \cdot \mathbf{p}) \tag{3.19a}$$

if

$$1/2(\mathbf{L}_k^T \cdot \mathbf{p})^2 + 1/2(\mathbf{L}_k^T \cdot \frac{\partial V}{\partial \mathbf{x}})^2 / \Omega_k^2 < 1/2\hbar\Omega_k. \tag{3.19b}$$

[It is not hard to show that Eq. (3.19a) corresponds to $P_k \rightarrow -P_k$ for mode k, and no change for all other modes.]

The model described above clearly does the job of not allowing the vibrational energy of any mode to dip below its zero point value. It is thus not possible for the zero point energy to "pool" in a single degree of freedom and cause unphysical behavior. Also, the imposition of the zero point energy constraint within a harmonic approximation should not be a serious limitation because the algorithm affects the classical mechanics only when the energy in a vibrational mode is near its zero point value, and most such degrees of freedom should be well described harmonically at this low level of excitation.

Various applications of this model are in progress to test its usefulness and reliability.

4. A Semiclassical Tunneling Model for use in Classical Trajectory Simulation

One of the most serious limitations of classical mechanics, which hinders its application to many interesting chemical problems, is its inability to describe tunneling effects. However the quantum mechanical phenomenon of tunneling is often quite prominent in chemical reactions that involve significant motion of light atoms. Typical examples include unimolecular dissociation or isomerization, e.g., the $H_2CO \rightarrow H_2 + CO$ decomposition, the isomerization reaction (1.1), as well as bimolecular reactions that involve H-atom transfer, e.g.,

$$H_2 + H \rightarrow H + H_2,$$

$$H_2 + F \rightarrow H + HF.$$

There do exist "rigorous" semiclassical theories that describe how classical trajectories tunnel e.g., classical S-matrix theory[23] and the "instanton" (periodic orbit in pure imaginary time) model,[24,25] but they are difficult to apply routinely to sizeable (e.g., more than three atom) molecular systems. There also exist a host of simple tunneling corrections to transition state theory[26] expressions for thermal rate constants; these often work well for this purpose, but they are not applicable to more general dynamical phenomena.

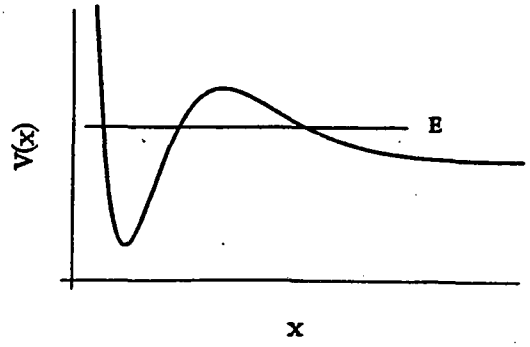

Figure 7. A typical one-dimensional potential for unimolecular decay. An energy level that corresponds to a quasi-bound state is indicated.

What we seek is a semiclassical model, as generally applicable as possible, for including tunneling in a classical trajectory simulation of the full molecular dynamics; the purpose of this paper is to present such a model. The model we have developed is similar in spirit to the Tully-Preston[27] surface hopping model for electronically non-adiabatic processes. In the Tully-Preston model a classical trajectory moving on one potential energy surface (i.e., Born-Oppenheimer electronic state) has a probability of making "hops", i.e., instantaneous transitions, to another potential energy surface at certain times. In the tunneling model presented herein the classical trajectory evolving in one classically allowed region of space will, at specific times, have a probability for making an instantaneous (in real time) transition to another classically allowed region of space. The model may also be viewed as the *classical* version of the semiclassical branching model of Waite and Miller,[28] but generalized to allow for a more general

tunneling path. This more general tunneling path is very closely related to that used by Heller and Brown[29] in their semiclassical treatment of radiationless transitions.

We first give a qualitative discussion/motivation for the model, and then define it more precisely. The results of some test calculations on model Hamiltonians illustrate some of its quantitative features. In general the model is seen to provide an excellent description of tunneling phenomena over a wide range of conditions (e.g., coupling constants, different symmetries of coupling).

4.1 ONE-DIMENSIONAL CASE

It is well known that the rate of unimolecular decay from a one-dimensional well, as in Figure 7, is given semiclassically (and accurately!) by[30]

$$k = \frac{\omega}{2\pi} e^{-2\theta}, \tag{4.1a}$$

where ω is the vibrational frequency in the well and $e^{-2\theta}$ is the probability of tunneling through the barrier; θ is the classical action integral through the barrier,

$$\theta = \frac{1}{\hbar} \mathrm{Im} \int_{\mathrm{barrier}} p(x)dx. \tag{4.1b}$$

Since $\omega/2\pi$ is the frequency that the trajectory experiences a classical turning point at the barrier, one may interpret Eq. (4.1) as a classical trajectory that oscillates in the well, tunneling out with probability $e^{-2\theta}$ every time it "hits" the barrier. If the particle is considered to be in the well at time t = 0, the *net probability that the particle has tunneled*, $P_{net}(t)$ is[31]

$$P_{net}(t) = \sum_n h(t - t_n)P_n, \tag{4.2a}$$

where $h(\xi)$ is the usual step function (= 1 if $\xi > 0$, = 0 if $\xi < 0$), t_n are the various "tunneling times," the times that the classical trajectory x(t) is at its outer turning point (i.e., "hits the barrier"), and

$$P_n = e^{-2\theta} \tag{4.2b}$$

is the tunneling probability for time t_n (here the same at each tunneling time). Figure 8 indicates the "staircase" character of $P_{net}(t)$. Averaging over the initial phase of the vibrational motion in the well will smooth out these steps, and it is not hard to see that the tunneling rate of Eq. (4.1a) is equivalently given by the slope of the averaged net tunneling probability $P_{net}(t)$, i.e.,

$$k = \frac{d}{dt}\langle P_{net}(t)\rangle. \tag{4.2c}$$

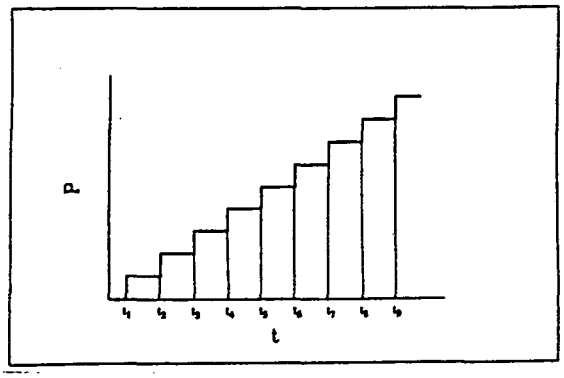

Figure 8. The net tunneling probability, $P_{net}(t)$, as a function of the time t, for a one dimensional potential of the type shown in Fig. 7. The "tunneling times" t_1, t_2,..., i.e., the times at which the trajectory experiences an outer turning point, are indicated.

The above discussion, which involves tunneling *probabilities*, applies to unimolecular dissociation, as pictured in Figure 7, and also to isomerization in an asymmetric double well potential that is irreversible on the time scale of physical interest. (Without the pre-exponential factor, it also gives the reaction probability for tunneling in bimolecular reactions, either symmetric or asymmetric.) The above description is *not* appropriate, however, to resonant tunneling in a *symmetric* double well potential, for the quantity of interest there, the splitting of the two degenerate energy levels, involves the tunneling amplitude.[30,32] For the present one-dimensional case this tunneling splitting is given semiclassically by

$$\Delta E = \frac{\hbar\omega}{\pi} e^{-\theta}, \tag{4.3a}$$

where ω and θ are the same quantities as above. Following the same analysis as in the

preceding paragraph, however, one can express ΔE in terms of the *net tunneling amplitude*

$$S_{net}(t) = \sum_n h(t - t_n)S_n, \tag{4.3b}$$

$$S_n = e^{-\theta}, \tag{4.3c}$$

as follows:

$$\Delta E = 2\hbar \frac{d}{dt}\langle S_{net}(t)\rangle, \tag{4.3d}$$

where the bracket implies an average over the initial phase of vibrational motion. We note that the same relation, Eq.(4.3d), also results from first order time dependent perturbation theory, whereby one has (to within a constant phase factor)

$$S(t) = H_{ab}\, t/\hbar,$$

$$\Delta E = 2H_{ab}$$

where H_{ab} is the exchange matrix element between states localized in wells "a" and "b".

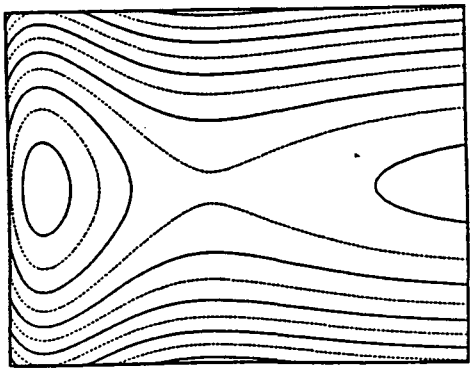

Figure 9. Contour plot of a separable two-dimensional potential. The potential in the s coordinate is that of Fig. 1, while the Q coordinate is a simple harmonic oscillator.

4.2 SEPARABLE MULTIDIMENSIONAL CASE

Now consider a separable N-dimensional potential

$$V(s,Q_1,\ldots,Q_{N-1}) = V_0(s) + \sum_{i=1}^{N-1} V_i(Q_i), \tag{4.4}$$

where the potential for the s coordinate has a barrier, and the potentials V_i are simple oscillators. Figure 9 shows a contour plot of such a potential for N=2, and a classical trajectory for energy E below the top of the barrier is shown in Figure 10a. A separable potential is a special case of an integrable system, with the N constants of the motion E_i, i=1,...,N specified by energy conservation in each degree of freedom individually. All trajectories that correspond to the same constants of the motion are confined on an N-dimensional manifold embedded in 2N-dimensional phase space. If the motion is bounded, this manifold has the topology of a torus and its projection onto configuration space is an N-dimensional parallel piped (a "box"), with the sides (caustic surfaces) traced out by the trajectories as they go through turning points in each degree of freedom. A typical trajectory gives rise to a Lissajous-type figure (see Figure 10a). For N=2, the trajectory manifold touches the boundary of the energetically allowed region at four points, the "corners".

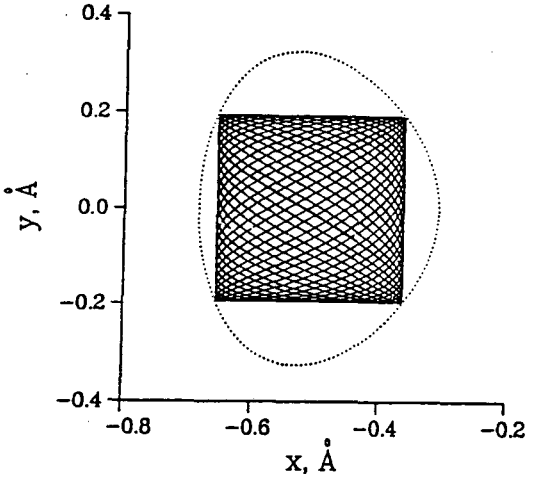

Figure 10a. A trajectory corresponding to the semiclassical ground state of a separable two-dimensional potential. The trajectory (or a set of trajectories that correspond to the same semiclassical state) defines a rectangular region bounded by the caustics. The dotted line shows the energy contour.

Since the potential is separable, tunneling involves only the s degree of freedom and is described as in Section IIa. Thus, the tunneling times $\{t_n\}$ occur whenever the s degree of freedom experiences an outer turning point, and the tunneling path is a straight line — the s axis — perpendicular to the trajectory at time t_n. The passage through the barrier takes place in pure imaginary time, during which the N-1 momenta $P_1,...,P_{N-1}$ remain constant. The decay rate is the same as that of the one-dimensional potential V_0, i.e., given by Eq. (4.2). Note that the action integral is

$$\theta = \frac{1}{\hbar}\mathrm{Im}\int p_s ds = \frac{1}{\hbar}\mathrm{Im}\int_{\text{tunneling path}} \mathbf{p}\cdot d\mathbf{q}, \tag{4.5}$$

where

$$\mathbf{q} \equiv (s,Q_1,...,Q_{N-1}) \text{ and } \mathbf{p} \equiv (p_s,P_1,...,P_{N-1}).$$

Finally we note that the trajectory reaches the products region with the same momentum $\mathbf{p}$ with which it began to tunnel and at the *same real time* (i.e., the tunneling involves only a pure imaginary time increment). The semiclassical picture is thus that the tunneling process is instantaneous (in real time) and conserves the momentum $\mathbf{p}$.

4.3 GENERAL (NON-SEPARABLE) CASE

We consider a generic Cartesian Hamiltonian

$$H(\mathbf{q},\mathbf{p}) = \sum_{i=1}^{N} \frac{p_i^2}{2m} + V(\mathbf{q}), \tag{4.6}$$

where the potential function V is in general non-separable. The above tunneling model is generalized by allowing the trajectory to tunnel along a *straight line path* in a specified direction $\hat{\mathbf{n}}_0$, every time the component of the momentum $\mathbf{p}$ along $\hat{\mathbf{n}}_0$, $\mathbf{p}\cdot\hat{\mathbf{n}}_0$, experiences a classical turning point (i.e., goes through zero) in the outward direction; equivalently, this corresponds to the times that the component of the coordinate vector $\mathbf{q}$ along the direction $\hat{\mathbf{n}}_0$, $\mathbf{q}\cdot\hat{\mathbf{n}}_0$, goes through a relative maximum.

The choice of the tunneling direction $\hat{\mathbf{n}}_0$ will be discussed more fully below. Requiring the tunneling path to be a straight line (in the full dimensional coordinate

space) is, of course, an approximation in the general non-separable case, but a reasonable one. Calculations based on the more rigorous classical S-matrix[23] and "instanton" [24,25] theories show that the optimum tunneling path is relatively straight in the tunneling region.

To describe the tunneling model more specifically, it is useful to make a change of coordinates (a point transformation) $\{q_i\} \rightarrow \{x,y_1,...,y_{N-1}\}$, where x is the component of **q** along the tunneling path,

$$x = \mathbf{q}\cdot\hat{\mathbf{n}}_0 \tag{4.7}$$

and $\{y_1,... y_{N-1}\}$ define N-1 orthogonal directions perpendicular to $\hat{\mathbf{n}}_0$. The Hamiltonian is then expressed in the new coordinate system:

$$\tilde{H}(x,y,p_x,\mathbf{p}_y) = \frac{p_x^2}{2m} + \sum_{i=1}^{N-1} \frac{p_{y_i}^2}{2m} + \tilde{V}(x,y), \tag{4.8}$$

where $\mathbf{y} \equiv (y_1,...,y_{N-1})$ and $\mathbf{p}_y$ is the vector of conjugate momenta. Since by our choice of tunneling path all components of **y** and $\mathbf{p}_y$ remain constant during the straight line tunneling process, the tunneling integral is given by

$$\theta = \frac{1}{\hbar}\,\mathrm{Im}\int_{\text{tunneling path}} \mathbf{p}\cdot d\mathbf{q} = \frac{1}{\hbar}\,\mathrm{Im}\int p_x dx. \tag{4.9}$$

Furthermore, due to energy conservation along the tunneling path, we have

$$\frac{p_x(t)^2}{2m} + \frac{\mathbf{p}_y(t)^2}{2m} + \tilde{V}[x(t),y(t)] = \frac{p_x(t_0)^2}{2m} + \frac{\mathbf{p}_y(t_0)^2}{2m} + \tilde{V}(x_0,y_0) \tag{4.10}$$

where (x_0,y_0) are the coordinates of the trajectory at the tunneling time t_0, and $t\text{-}t_0$ is pure imaginary. But $p_x(t_0) = 0$, $\mathbf{p}_y(t) = \mathbf{p}_y(t_0)$, and $\mathbf{y}(t) = \mathbf{y}_0$, so we obtain

$$p_x = i\sqrt{2m[\tilde{V}(x,y) - \tilde{V}(x_0,y_0)]} = i\sqrt{2m\{V[\mathbf{q}_0 + (x\text{-}x_0)\hat{\mathbf{n}}_0] - V(\mathbf{q}_0)\}}. \tag{4.11}$$

The tunneling integral is thus given

$$\theta_0 = \frac{1}{\hbar}\int_0^{\xi_{max}} \sqrt{2m[V(q_0 + \xi\hat{n}_0) - V(q_0)]}\, d\xi \tag{4.12}$$

and the probability for tunneling at time t_0 is

$$P_0 = e^{-2\theta_0}, \tag{4.13}$$

where ξ_{max} is the value of ξ at which the integrand of Eq. (4.12) equals zero, i.e., the value for which the tunneling trajectory reaches another classically allowed region of space.

It is useful to emphasize that the above algorithm is easily implemented in the original coordinates and momenta $(\mathbf{q},\mathbf{p})$ of Eq. (4.6) without actually having to make the canonical transformation used above to describe it. Thus one monitors the quantity x(t) of Eq. (4.7) while the trajectory $(\mathbf{q}(t), \mathbf{p}(t))$ is being computed; t_0 is a time at which x(t) experiences a local maximum, and $\mathbf{q}_0 \equiv \mathbf{q}(t_0)$, $\mathbf{p}_0 \equiv \mathbf{p}(t_0)$. The tunneling integral is then given by Eq. (4.12), where ξ_{max} is the value of the integration variable at which the integrand vanishes, and the tunneling probability is given by Eq. (4.13). (If the integrand of Eq. (4.12) never vanishes for $\xi>0$, then one has $\theta_0 \rightarrow +\infty$ and thus $P_0 \rightarrow 0$; i.e., the tunneling path never finds another classically allowed region.) If one wishes to follow the trajectory in the new classically allowed region — e.g., in order to determine the product state distribution — then the initial conditions for it are

$$\mathbf{q}_{new}(t_0) = \mathbf{q}_0 + \hat{\mathbf{n}}_0\xi_{max}, \tag{4.14a}$$

$$\mathbf{p}_{new}(t_0) = \mathbf{p}_0. \tag{4.14b}$$

4.4 CHOICE OF THE TUNNELING PATH

To complete the description of the model, we must specify the "tunneling direction" $\hat{\mathbf{n}}_0$ introduced in the preceding Section. We have actually investigated a variety of choices and describe here the one which has proved most satisfactory in general and which seems most justifiable on theoretical grounds.

Consider first the initial conditions for a trajectory in the reactant potential well. For

the semiclassical picture to be meaningful, we assume that the motion in the reactant potential well does not explore all energetically accessible regions of phase space, but is constrained to lie on an N-dimensional KAM torus,[33] as in the separable case, for the energy that corresponds to the desired initial conditions. This is a reasonable assumption, especially if one is interested in tunneling from low lying initial states (e.g., from the ground state). More specifically, we will be considering trajectories that start out with initial conditions $(\phi,\mathbf{J})$ in action-angle variables,[33(a)] where the actions

$$J_i = \frac{1}{2\pi}\int_{\Gamma_i} \mathbf{p}\cdot d\mathbf{q} = (n_i + \frac{1}{4}\mu_i)\hbar \tag{4.15}$$

are defined along the N topologically distinct paths (basis contours) Γ_i on the torus and are quantized, and μ_i is the corresponding Maslov index.[34] Averaging over initial conditions then corresponds to averaging over the angles $\{\phi_i\}$, i=1,...,N. These are the polyatomic version of the standard quasiclassical initial conditions (EBK quantization).[35]

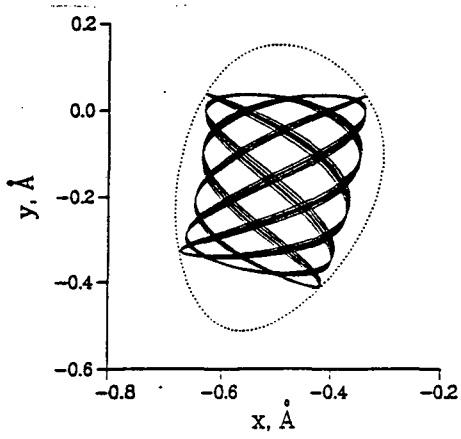

Figure 10b. A similar trajectory for a non-separable two-dimensional potential. The classical motion is regular, i.e., the trajectory lies on a KAM torus and will, over time, trace out two-dimensional region which is a subset of the energy shell. This region (the "trajectory manifold") is the projection of the KAM torus onto configuration space; it touches the energy contour at four points, the "corners", and is bounded by caustics. The dotted line shows the energy contour.

Since the motion is assumed to sweep out a torus, its projection onto configuration space still gives rise to "box"-like shapes (see Figure 10b). Unlike the separable case, the edges of such a "box" need no longer be straight lines, though one can show that they still cross at right angles near a comer;[36] i.e., the motion is locally separable about a

corner. We now employ the concept of the semiclassical wavefunctions that correspond to these box-like trajectories and a simple argument from quantum mechanics to motivate our choice of the tunneling path. Quantum mechanically, the amplitude for a transition from the initial state $|\psi_i\rangle$ to the final state $|\psi_f\rangle$ is given by

$$\langle\psi_f|\hat{T}|\psi_i\rangle,$$

where T is the appropriate transition operator, in our case the Hamiltonian. The semiclassical wavefunction in the region near the caustic surfaces but *outside* the trajectory manifold can be defined (by generalizing the well known one-dimensional WKB results) as the analytic continuation of the WKB wavefunction on the manifold.[37] The wavefunction will be proportional to the exponential of a properly defined action integral, and is largest near the edges of the manifold. The tunneling amplitude accumulates its magnitude from the regions of space where the initial and final state wavefunctions overlap the most. The overlap of these wavefunctions is clearly maximized along the shortest straight line that joins these manifolds. We thus choose the tunneling direction $\hat{\mathbf{n}}_0$ as *the straight line that connects the manifolds* that correspond to the initial and final state *in the shortest possible way*. Figure 11 shows three typical cases, and the tunneling path for each case.

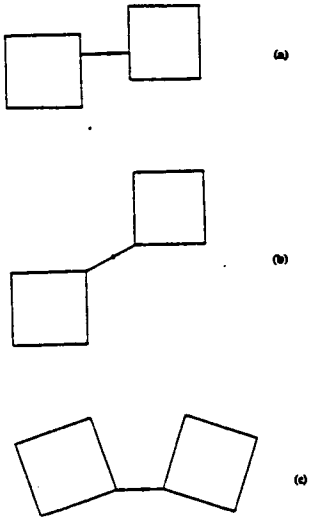

Figure 11. The boundary of the trajectory manifolds and the "tunneling path" according to the definition of Section 4.5 in three typical cases.

We note that the above choice for the tunneling direction is the same in spirit as that of Heller and Brown[29] in their treatment of semiclassical matrix elements for radiationless transitions. The primary difference is that our model does not restrict tunneling only to the "corner to corner" (or corner to edge) path, but allows for tunneling in the "corner to corner" *direction* every time the component of the motion along this direction experiences a classical turning point. We also note that this "corner to corner" tunneling direction is also very similar to that yielded in some applications of "rigorous" semiclassical theories, i.e., classical S-matrix theory[23] and the instanton model.[24,25]

4.5. APPLICATION: TUNNELING RATES IN MODEL POTENTIALS

We envision the present model to be most useful for describing tunneling processes in complex molecular systems involving unimolecular decomposition and isomerization. To provide a qualitative test, however, here we show how it performs on some simple two-dimensional Hamiltonians of the following form

$$H = \frac{p_s^2}{2m} + \frac{p_Q^2}{2m} + V(s,Q). \tag{4.16}$$

We performed calculations of the tunneling splitting in symmetric double wells and of unimolecular decay rates from quasi-bound initial states. The specific form of the model potential that we used for this application is the same as that in our earlier papers,[15]

$$V(s,Q) = V_0(s) + \frac{1}{2} m\omega^2 \left[Q - \frac{f(s)}{m\omega^2} \right]^2 . \tag{4.17a}$$

Here s is the reaction coordinate, $V_0(s)$ is a symmetric double well,

$$V_0(s) = -\frac{1}{2} a_0 s^2 + \frac{1}{4} c_0 s^4, \tag{4.17b}$$

f(s) is the coupling function, and Q is the orthogonal harmonic degree of freedom, which is linearly coupled to the reaction coordinate. Notice that the term $[f(s)]^2/2m\omega^2$ in Eq. (4.17a) renormalizes the height of the barrier so that it is independent of the strength of the coupling, and the dependence of the tunneling splitting on the coupling is merely due

to the distortion of the potential surface away from the separable case. The constants were chosen such that the barrier height is 7.8 kcal/mol and the two potential minima are located at $s_{\pm} = \pm 0.53$Å. The mass was chosen to be that of a hydrogen atom, and the frequency of the harmonic oscillator was 298 cm^{-1}. These parameters are the same as those in Ref. 15 and are typical of H-atom transfer processes.

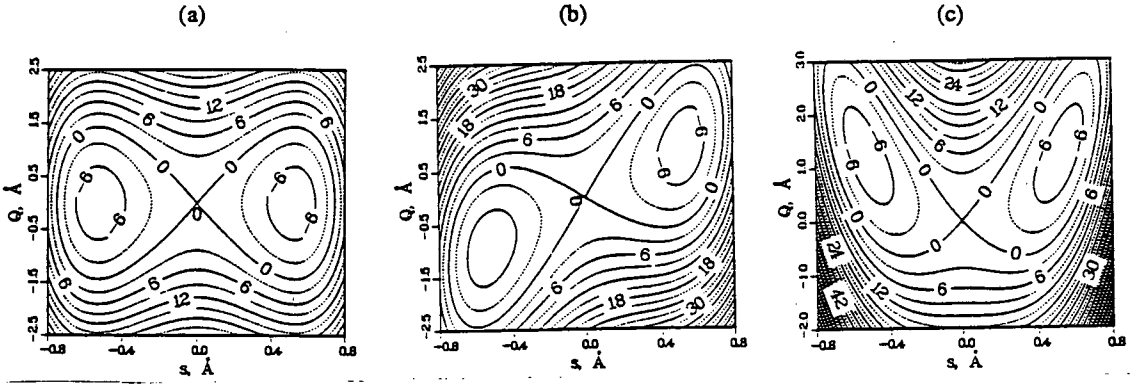

Figure 12. Contour plot of the two-dimensional potential used in the calculations [cf. Eq. (4.17)]. The potential in the s coordinate is a symmetric double well, while the Q coordinate is a harmonic oscillator of frequency 298 cm^{-1}. (a) Separable case (c=0); (b) Linear coupling, f(s)=cs, for c=0.004 hartree/$bohr^2$; (c) Quadratic coupling, $f(s)=cs^2$, for c=0.004 hartree/$bohr^3$.

We considered two different forms of the coupling function f(s) which give rise to different symmetries in the full (coupled) potential: (i) linear coupling, f(s)=cs, for which V possesses inversion symmetry, and (ii) quadratic coupling, $f(s)=cs^2$, in which case V has reflection symmetry with respect to the Q axis. Figure 12 shows contour plots of the potential in these two different cases for typical values of the coupling constant c.

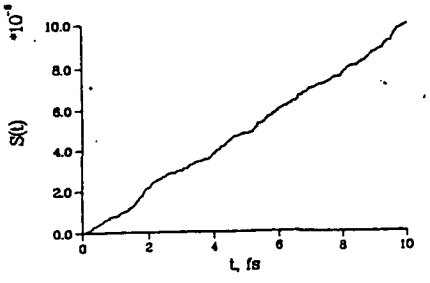

Figure 13. The net tunneling amplitude [cf. Eq. (2.3a)], averaged over 1000 trajectories, for a trajectory in the potential of Fig. 12b.

In the case of linear coupling, the two wells move apart in the Q direction as the coupling increases. For small values of c, our rule for choosing the tunneling path gives $\hat{n}_0 = \hat{s}$, i.e., the trajectories tunnel purely in the s direction (cf. Figure 11a). As the coupling constant gets larger, however, the shortest line that connects the "boxes" becomes the line that connects the nearest corners passing through the transition state (cf. Figure 11b). In the case of quadratic coupling, the tunneling path is always the line that connects the nearest corners, which is in this case the s direction (cf. Figure 11c).

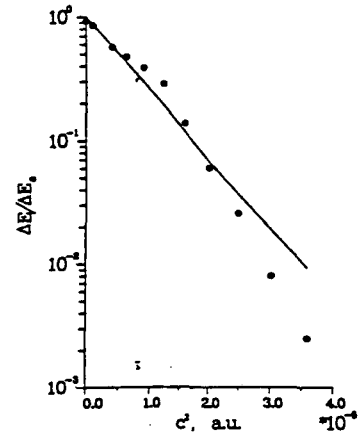

Figure 14. The tunneling splitting ΔE, normalized by the exact quantum value ΔE_0 of the splitting in the one-dimensional double well, as a function of the square of the coupling constant c, for the case of linear coupling, f(s)=cs. Solid line: exact quantum results, obtained by a basis set calculation. Circles: results obtained by using the semiclassical model presented in this paper.

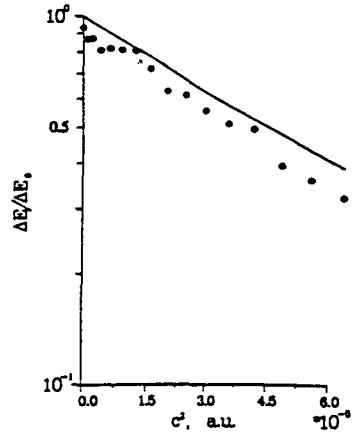

Figure 15. Same as Fig. 14, except for quadratic coupling $f(s)=cs^2$.

Since the double well is symmetric, we use the amplitude version of the model, as described at the end of Sec. 4.1. Figure 13 shows a typical graph of the net tunneling amplitude $S_{net}(t)$ defined by Eq. (4.3b), with $S_n = e^{-\theta_n}$, averaged over 1000 trajectories. The linear character of this function is obvious, and the slope gives the tunneling splitting according to Eq. (4.3c). Figures 14 and 15 show the tunneling splitting ΔE as given by this semiclassical model, normalized by the exact (quantum) value ΔE_0 of the tunneling splitting at zero coupling, as a function of the square of the coupling constant c, for the cases of linear and quadratic coupling. Also shown are the exact quantum mechanical values of $\Delta E/\Delta E_0$, obtained by numerical diagonalization of the Hamiltonian in a basis set. The agreement between the semiclassical results and the exact ones is quite good, even when the coupling is very strong.

In a real molecular system, e.g., Eq. (1.1), there will of course be some modes most akin to the even coupling case above (e.g., the O-O stretch mode in Eq. (1.1) and other modes that are typified by the odd coupling use [e.g., a C-O stretch mode in (1.1)]. The fact that the above semiclassical model is able to describe the effect of coupling on the tunneling dynamics for both kinds of modes suggests that it may be of useful generality for more complex molecular systems.

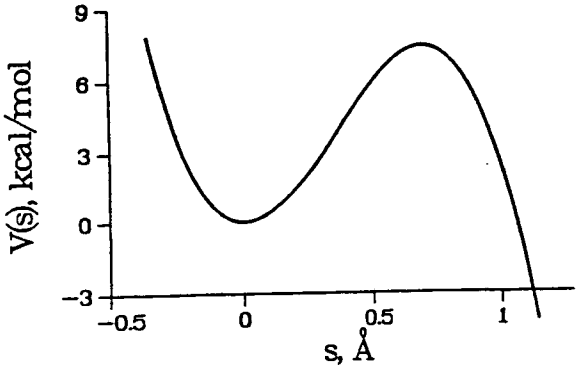

Figure 16. The potential V_0 which was used in the calculation of the unimolecular decay rate [cf. Eq. (4.18b)].

Finally, we apply the tunneling model (the probability version of it) to calculate the decay rate from the ground quasibound state (i.e., lowest energy resonance) of a two-dimensional potential which has the form

$$V(s,Q) = V_0(s) + 1/2m\omega^2Q^2 - csQ, \qquad (4.18a)$$

$$V_0(s) = 1/2a_0s^2 - 1/3b_0s^3. \qquad (4.18b)$$

The one-dimensional potential V_0 is shown in Figure 16; the local maximum occurs at s=0.71Å and the barrier height is 7.4 kcal/mol. The mass was chosen to be that of a hydrogen atom, and the frequency of the harmonic oscillator was 298 cm^{-1}. Figure 17 shows a contour plot of the two-dimensional potential for a typical value of the coupling parameter c. The semiclassical decay rate was calculated according to Eq. (4.2).

In order to generate accurate quantum mechanical results for comparison, we computed the width of the resonance using the method of complex scaling.[38] The s coordinate was rotated as $s \rightarrow se^{i\alpha}$, while the Q coordinate remained real. The complex scaled Hamiltonian was then diagonalized in a basis set of (real) particle in a box basis functions and the complex eigenvalues

$$E = E_R + iE_I \qquad (4.19a)$$

which were stable under a change of the scaling angle α were identified as resonances, whose width is

$$\Gamma = -2E_I. \qquad (4.19b)$$

The decay rate k is obtained in terms of the resonance width according to

$$k = \frac{\Gamma}{\hbar}. \qquad (4.19c)$$

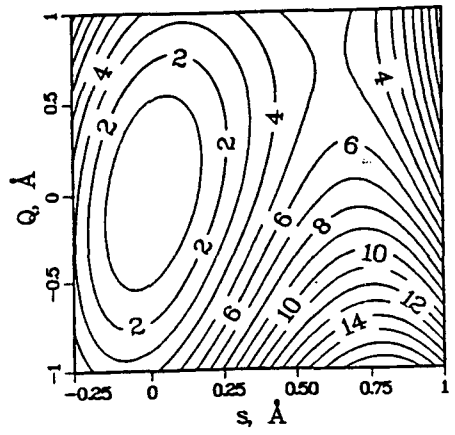

Figure 17. Contour of the two-dimensional potential Eq. 4.18, for c=0.004 hartree/$bohr^2$. The potential in the s coordinate is shown in Fig. 16, while the Q coordinates is a harmonic oscillator of frequency 298 cm^{-1}.

Figure 18 compares the results of the semiclassical model for the decay rate with the quantum mechanical ones, i.e., those of the complex scaling calculation. Plotted is the

decay rate k (normalized by the exact quantum value of the rate for the uncoupled potential) as a function of the square of the coupling constant c. The agreement is of the same quality as in the previous applications — within a factor of 2 in the worst case, while the coupling is so strong that it has increased the value of k by two orders of magnitude.

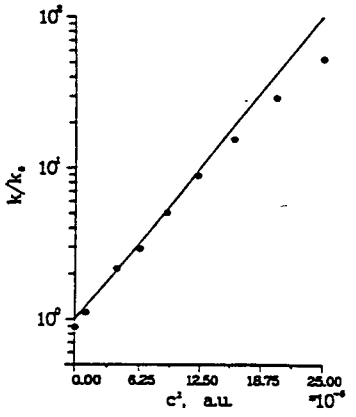

Figure 18. The decay rate k, normalized by the exact quantum value k_0 of the rate in the one-dimensional potential V_0, as a function of the square of the coupling constant c. Solid line: exact quantum results, obtained by the method of complex scaling. Circles: results obtained by using the semiclassical model described in this paper.

5. Concluding Remarks

This lecture has described recent advances regarding three specific aspects of chemical reaction dynamics in polyatomic molecular systems. First, it was seen how the empirical valence bond idea can be used to combine the popular empirical potential energy functions, which do a good job of describing *non-reactive* molecular motions, with *ab initio* calculations of the transition state properties of a reactive system and in a simple way obtain a *global* potential energy function for the reacting systems. Applications to test problems suggests that this model is flexible and provides a semi-quantitative description in a variety of situations. Recent applications to the formaldehyde dissociation

$$H_2CO \rightarrow H_2+CO$$

has given an excellent description of this reaction.

Second, it was shown how a relatively simple procedure can be used to correct

(approximately) classical trajectories for zero point energy effects. This model prevents the vibrational energy in each individual mode from dropping below its instantaneous zero point value and thus prevents unphysical effects that could result otherwise. Finally, a very general semiclassical model was described for including quantum tunneling effects (approximately) in a classical trajectory simulation. Applications of this model to a variety of examples showed the model to be quite accurate in a variety of topologically different situations.

All of these methodologies should be applicable (in some form) to carrying out theoretical simulations of reaction dynamics in biomolecular systems.

Acknowledgment

This work has been supported by the Director, Office of Energy Research, Office of Basic Energy Sciences, Chemical Sciences Division of the U.S. Department of Energy under Contract No. DE-AC03-76SF00098.

References

1. Good overviews of the problem of representing potential energy surfaces are the reviews (a) D. G. Truhlar, R. Steckler, and M. S. Gordon, Chem. Rev. 87, 217 (1987); and (b) G. C. Schatz, Rev. Mod. Phys. 61, 669 (1989).
2. See, for example, W. J. Hehre, L. Radom, P. v. R. Schleyer, and J. A. Pople, Ab Initio Molecular Orbital Theory, Wiley, N.Y., 1986.
3. R. A. Marcus, J. Chem. Phys. 49, 2610 (1968).
4. (a) W. H. Miller, N. C. Handy and J. E. Adams, J. Chem. Phys. 72, 788 (1980).
   (b) W. H. Miller, J. Phys. Chem. 87, 3811 (1983).
5. K. Fukui, Acct. Chem. Res. 14, 363 (1981).
6. J. T. Hougen, P. R. Bunker, and J. W. C. Johns, J. Mol. Spectrosc. 34, 136 (1970).

7. (a) B. A. Ruf and W. H. Miller, J. Chem. Soc. Faraday Trans. 2 84, 1523 (1988).
   (b) W. H. Miller, B. A. Ruf, and Y.-T. Chang, J. Chem. Phys. 89, 6298 (1988).
8. (a) N. L. Allinger, J. Am. Chem. Soc. 99, 8127 (1977).
   (b) N. L. Allinger, Y. H. Yuh, and J.-H. Lii, J. Am. Chem. Soc. 111, 8551 (1989).
   (c) J.-H. Lii and N. L. Allinger, J. Am. Chem. Soc. 111, 8566 (1989).
   (d) J.-H. Lii and N. L. Allinger, J. Am. Chem. Soc. 111, 8576 (1989).
9. B. R. Brooks, R. E. Bruccoleri, B. D. Olafson, D. J. States, S. Swaminathan, and M. Karplus, J. Comput. Chem. 4, 187 (1983).
10. (a) P. K. Weiner and P. A. Kollman, J. Comput. Chem. 2, 287 (1981).
    (b) S. J. Weiner, P. A. Kollman, D. A. Case, U. C. Singh, C. Ghio, G. Alagona, S. Profeta, Jr., and P. Weiner, J. Am. Chem. Soc. 106, 765 (1984).
    (c) S. J. Weiner, P. A. Kollman, D. T. Nguyen, and D. A. Case, J. Comput. Chem. 7, 230 (1986).
11. W. L. Jorgensen and J. Tirado-Rives, J. Am. Chem. Soc. 110, 1657 (1988).
12. (a) A. Warshel and S. Lifson, J. Chem. Phys. 49, 5116 (1968).
    (b) A. Warshel, in Modern Theoretical Chemistry, Vol. 7, ed. G. A. Segal, Plenum, 1977, p. 133.
13. (a) A. Warshel and R. M. Weiss, J. Am. Chem. Soc. 102 6218 (1980).
    (b) A. Warshel, Biochemistry 20, 3167 (1981).
    (c) A. Warshel, Acc. Chem. Res. 14, 284 (1981).
14. See, for example, R. Kubo, J. Phys. Soc. Japan 17, 1100 (1962).
15. N. Makri and W. H. Miller, J. Chem. Phys. 86, 1451 (1987); 87, 5781 (1987); 91, 4026 (1989).
16. R. A. Marcus, Ber. Bunsenges. Phys. Chem. 81, 190 (1977) .
17. W. L. Hase and D. G. Buckowski, J. Comput. Chem. 3, 335 (1982).
18. G. C. Schatz, J. Chem. Phys. 79, 5386 (1983) .
19. For review, see
    (a) R. N. Porter and L. M. Raff, in Dynamics of Molecular Collisions, B, ed. W. H. Miller, Plenum, NY, 1976, p. 1;
    (b) L. M. Raff and D. L. Thompson, in Theory of Chemical Reaction Dynamics, Vol. III, ed. M. Baer, CRC Press, Boca Raton, FL, 1985, p. 1.

20. See, for example, J. M. Bowman, G. C. Schatz, and A. Kuppermann, Chem. Phys. Lett. 24, 378 (1974) .
21. D.-H. Lu and W. L. Hase, J. Chem. Phys. 89, 6723 (1988).
22. D.-H. Lu and W. L. Hase, J. Chem. Phys., submitted.
23. W. H. Miller, (a) Adv. Chem. Phys. 25, 69 (1974); (b) *ibid* 30, 74 (1975); (c) Science 233, 171 (1986).
24. W. H. Miller, J. Chem. Phys. 62, 1899 (1975).
25. (a) S. Colemam, Uses of Instantons, in The Whys of Subnuclear Physics, edited by A. Zichichi, Plenum, N.Y., 1979, pp. 805-916;
    (b) A. 0. Caldiera and A. J. Leggett, Ann. Phys. (N.Y.) 149, 374 (1983).
26. Some examples are:
    (a) D. G. Truhlar and B. C. Garrett, Ann. Rev. Phys. Chem. 35, 159 (1984);
    (b) G. C. Lynch, D. G. Truhlar, and B. C. Garrett, J. Chem. Phys. 90, 3102 (1989);
    (c) R. A. Marcus and M. E. Coltrin, J. Chem. Phys. 67, 2609 (1977);
    (d) C. J. Cerjan, S. Shi, and W. H. Miller, J. Phys. Chem. 86, 2244 (1982).
27. J. C. Tully and R. K. Preston, J. Chem. Phys. 55, 562 (1971).
28. B. A. Waite and W. H. Miller, J. Chem. Phys. 76, 2412 (1982).
29. E. J. Heller and R. C. Brown, J. Chem. Phys. 79, 3336 (1983).
30. See, for example, K. W. Ford, D. L. Hill, M. Wakano, and J. A. Wheeler, Ann. Phys. (N.Y.) 7, 239 (1959).
31. Eq. (4.2a) is correct for small tunneling probabilities, $P_n \ll 1$. More generally, one must include a "survival probability" factor, so that Eq. (4.2a) becomes
    $P_{net}(t) = \sum_{n=1} h(t - t_n)P_n$, where $p_1=P_1$ and $p_n=P_n x\left[1- \sum_{n'=1}^{n-1} P_{n'}\right]$ for $n>1$.
32. Also see the discussion by W. H. Miller, J. Phys. Chem. 83, 960 (1979).
33. (a) A. J. Lichtenberg and M. A. Lieberman, Regular and Stochastic Motion (Springer, New York, 1983);
    (b) M. V. Berry, Regular and irregular motion, in Topics in Nonlinear Dynamics, S. Joma, ed. A.I.P. Conference Proceedings 46, 1976; V. I. Arnold, Mathematical Methods of Classical Mechanics (Springer, New York, 1978).
34. V. P. Maslov and M. V. Fedoriuk, Semiclassical Approximation in Quantum Mechanics, (Reidel, Boston, 1981).

35. (a) A. Einstein, Verh. Dtsch. Phys. Ges. 19, 82 (1917);
(b) M. L. Brillouin, J. Phys. 7, 353 (1926);
(c) J. B. Keller, Ann. Phys. 4, 180 (1958).
36. P. Pechukas, J. Chem. Phys. 57, 5577 (1972).
37. (a) M. Wilkinson, Physica 21D, 341(1986);
(b) N. De Leon and E. J. Heller, Phys. Rev. A 30, 5 (1984).
38. (a) B. R. Junker, Adv. Atom. Mol. Phys. 18, 207 (1982);
(b) W. P. Reinhardt, Ann. Rev. Phys. Chem. 33, 223 (1982);
(c) B. A. Waite and W. H. Miller, J. Chem. Phys. 74, 3910 (1981).

LAWRENCE BERKELEY LABORATORY
UNIVERSITY OF CALIFORNIA
INFORMATION RESOURCES DEPARTMENT
BERKELEY, CALIFORNIA 94720